# Studies of $Nb_3Sn$ Strands based on the Restacked-Rod Process for High-field Accelerator Magnets

E. Barzi, M. Bossert, G. Gallo, V. Lombardo, D. Turrioni, R. Yamada, and A.V. Zlobin

***Abstract*—A major thrust in Fermilab's accelerator magnet R&D program is the development of $Nb_3Sn$ wires which meet target requirements for high field magnets, such as high critical current density, low effective filament size, and the capability to withstand the cabling process. The performance of a number of strands with 150/169 restack design produced by Oxford Superconducting Technology was studied for round and deformed wires. To optimize the maximum plastic strain, finite element modeling was also used as an aid in the design. Results of mechanical, transport and metallographic analyses are presented for round and deformed wires.**

***Index Terms*— $Nb_3Sn$, subelement, deformation, flux jumps**

## I. INTRODUCTION

To offer some margin to flux jump instabilities for $Nb_3Sn$ superconducting wires to be used in magnets, where the conductor sees deformations in the plastic regime, it is important to reduce as much as possible the superconducting subelement size. It was shown already [1] that Restacked-Rod Process (RRP) designs with 127 restacks and 0.7 mm size with extra Cu between the superconducting bundles withstand the cabling process and allow using the full current capacity of the conductor in magnets, at least at 4.2 K. This wire is presently a baseline conductor for $Nb_3Sn$ magnet R&D in the US [2]. However, it is clear that at the LHC operation temperature of 1.9 K, at which the conductor exhibits a much larger critical current density $J_c$, these wires still operate on the verge of instability.

In this paper the transport properties of 150/169 RRP wires of various sizes are measured. Then a comparison study was performed between the 150/169 and the baseline 108/127 design for 1 mm wires under deformation through flat rolling, which produces a homogenous deformation along the length of the strand. Wire deformation was defined as $(d_0\text{-}t)/d_0$, where $d_0$ is the original strand diameter and t the thickness of the deformed strand (Fig. 9). The study compares the effect of increasing deformation on the critical current, $I_c$, the stability current, $I_S$, and the residual resistivity ratio, RRR, between the two designs. An ANSYS finite element model validated with experimental data was then implemented to simulate plastic deformation of both strand designs.

Manuscript received 12 September 2011. This work was supported by the U.S. Department of Energy.

Authors are with the Fermi National Accelerator Laboratory (Fermilab), P.O. Box 500, Batavia, IL 60510 USA (phone: 630-840-3446; fax: 630-840-3369; e-mail: barzi@fnal.gov.

## II. EXPERIMENTAL SETUP

### A. Strand Description

Table I shows parameters of the 150/169 RRP (RRP1) and of the 108/127 RRP (RRP2) strands. Pictures of the cross sections are in Fig. 1. With the nominal heat treatment, the 1 mm RRP1 strand produced a $J_c$(4.2 K, 14 T) of 2643 A/mm$^2$, and the 0.7 mm wire a $J_c$(4.2 K, 14 T) of 2518 A/mm$^2$, as measured by OST.

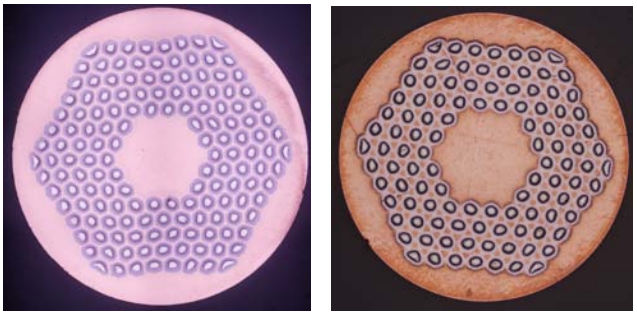

Fig. 1. 150/169 (left), and 108/127 (right) RRP designs used in this study.

TABLE I STRAND DESCRIPTION

| Strand ID | RRP1 | RRP2 |
|---|---|---|
| Stack design | 150/169 | 108/127 |
| Strand diameters, mm | 0.7, 0.8, 0.9, 1.0 | 0.7, 1.0 |
| $J_c$(4.2K, 12 T), A/mm$^2$ | > 2,400 | > 2,650 |
| Max subelement size, μm | 36-52 | 52-75 |
| Twist pitch, mm | 14 | 12 |
| Cu fraction, % | 51 | 54 |

### B. Sample Preparation and Measurement Procedure

The round and deformed strand samples were wound and heat treated in Argon atmosphere on grooved cylindrical barrels made of Ti-alloy. All the strands used in this study were given the same heat treatment schedule of 25°C/h up to 210°C, 48 h; 50°C/h up to 400°C, 48 h; 75°C/h up to 665°C, 50 h. After reaction, the samples were tested on the same barrel. The $I_c$ was determined from the voltage-current (V-I) curve using the $10^{-14}$ Ω·m resistivity criterion. The stability current, $I_S$, was obtained through V-H tests as the minimum quench current in the presence of a magnetic field variation. Stycast was used on the sample.

Operated by Fermi Research Alliance, LLC under Contract No. De-AC02-07CH11359 with the United States Department of Energy.

## III. Results and Discussion

### A. Comparison of Strand Performance at 4.2 K

Fig. 2 shows $J_c$(14 T) and $J_S$ of the RRP1 round strands as a function of the geometric subelement size $D_S$. Whereas the $J_c$(14 T) is similar for all round strands, Fig. 2 shows a clear some dependence of $J_S$ with $D_S$ whenever power supply limit (PSL in Figure) is not reached..

In Fig. 3 the $I_c$(14 T) of the rolled strand normalized to that of the 1 mm round strand is compared between the 150/169 and the 108/127 wires as function of wire deformation. Typical $I_c$ measurement uncertainties are within ±1% at 4.2 K and 12 T. It can be seen that up to 40% deformation the $I_c$(14 T) degrades similarly or less under increasing deformation in the 150/169 design. This is consistent with previous findings that smaller subelements are less sensitive to $I_c$ degradation [3].

In Fig. 4 the $J_c$(14 T) of the 150/169 and 108/127 1 mm strands are compared as function of wire deformation.

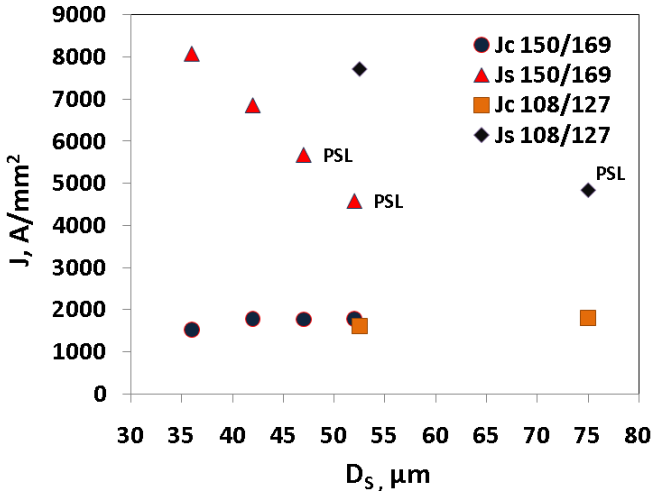


Fig. 2. $J_c$(14 T) and $J_S$ of the RRP1 round strand as a function of geometric subelement size.

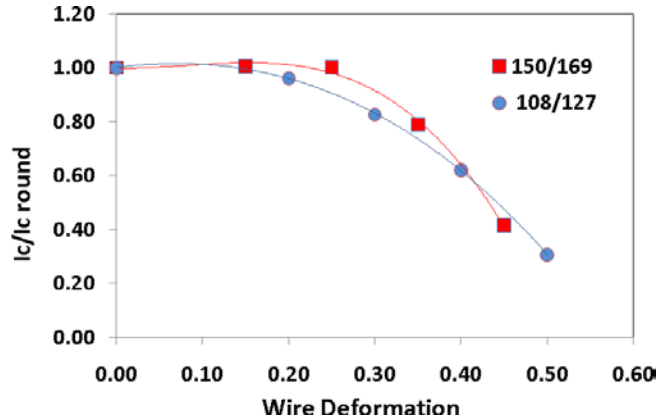


Fig. 3. $I_c$(14 T) of the rolled strand normalized to that of the round strand function of wire deformation for the 150/169 and 108/127 1 mm designs.

Figs. 5 and 6 show V-I and V-H test results of the 1 mm round and rolled strands with 150/169 and 108/127 restacks respectively. The power supply limits of the two test stations that were used are 1790 A and 2000 A as shown in the two Figures.

Fig. 7 shows the RRR comparison between the 150/169 and the 108/127 1 mm strand samples as function of wire deformation. It can be seen that the 150/169 strand has a systematically better $J_S$ performance over most of the deformation range, which is consistent with its subelements being 30% smaller. The deformed 1 mm 150/169 strand shows RRR values that are consistently larger than for the 108/127.

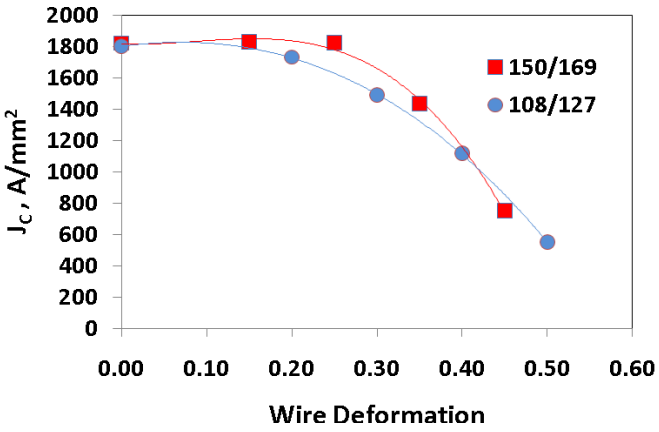


Fig. 4. The $J_c$(14 T) of the 150/169 and 108/127 1 mm strand designs are compared as function of wire deformation.

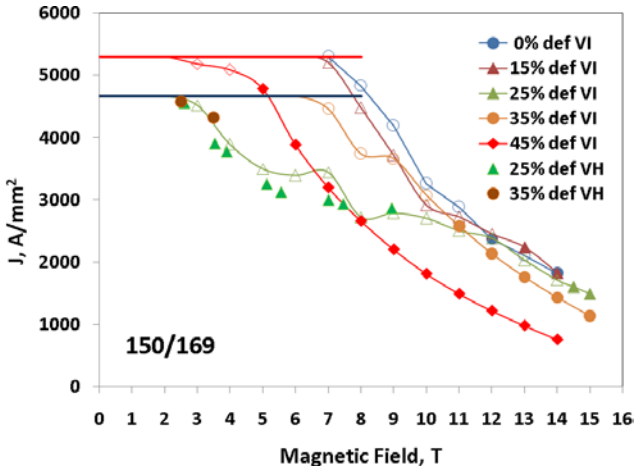


Fig. 5. V-I and V-H test results at 4.2 K for the 1 mm round and rolled strands with 150/169 restacks.

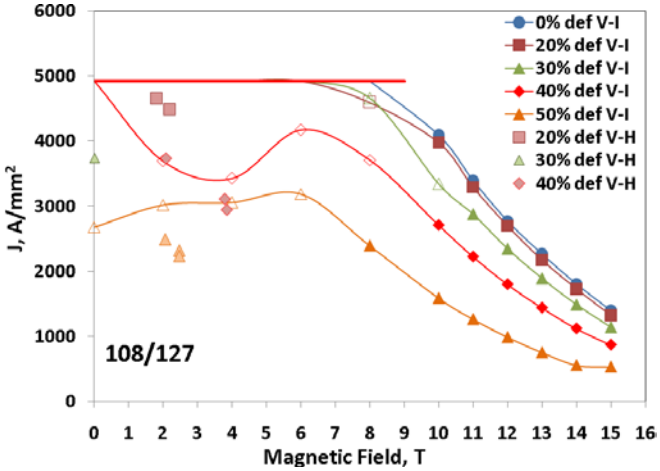


Fig. 6. V-I and V-H test results at 4.2 K for the 1 mm round and rolled strands with 108/127 restacks.

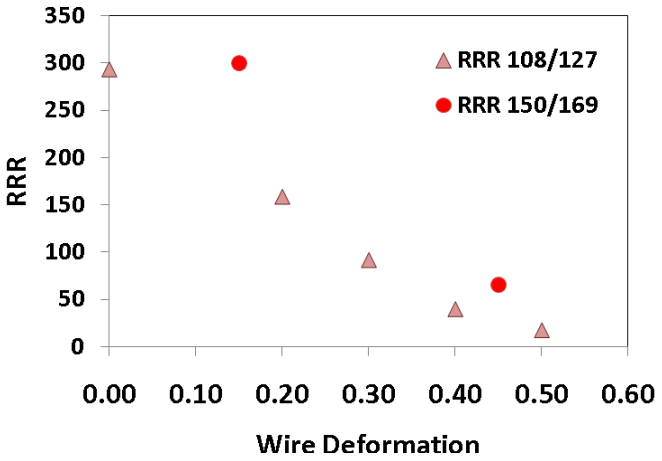


Fig. 7. The RRR of the 150/169 and 108/127 1 mm strands are compared as function of wire deformation.

### B. *Strand FEM Modeling*

To model strand deformation with ANSYS, a rigid contact surface was gradually applied to a round composite made of Sn and Nb hexagonal elements embedded in a Cu matrix [4]. A flexible contact element was used on the wire surface. Elastic and plastic material properties were used. The mesh was optimized in order to provide much finer information in the Cu channels between bundles, where failure occurs first. The model was validated through comparisons with a large statistics of deformed strand cross sections at each deformation stage. The present simulation procedure does not model fracture. However an excellent correlation was found with the data up to relative deformations of 26% [4]. Fig. 8 shows the two models used for the 150/169 (left) and the 108/127 [4] (right) strands.

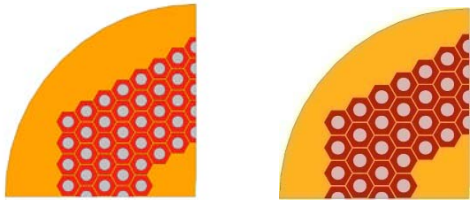

Fig. 8. Model geometry for RRP 150/169 (left) and 108/127 [4] (right) wires.

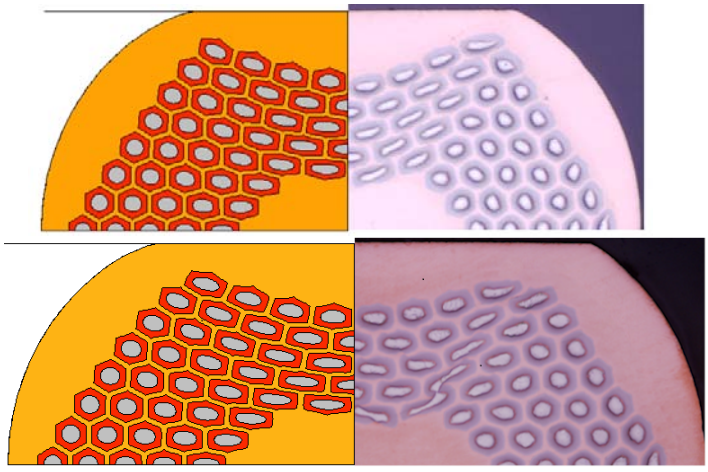

Fig. 9. ANSYS model results of plastic work for a 150/169 wire deformed by 20% (top) and by 25% (bottom).

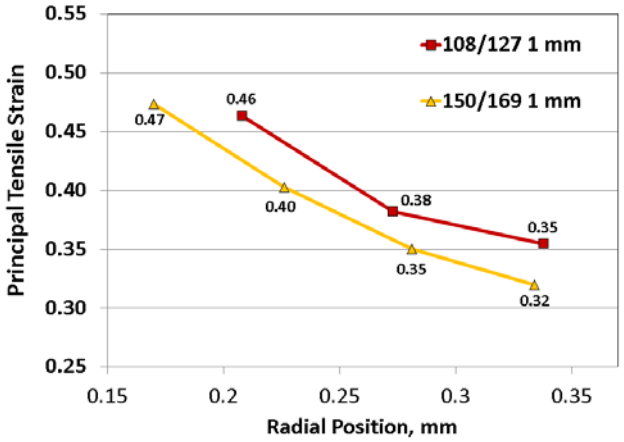


Fig. 10. Principal tensile strain in the Cu along the 2nd diagonal at 26% deformation as a function of radial position for the 1 mm 150/169 and 108/127 [4] strand designs.

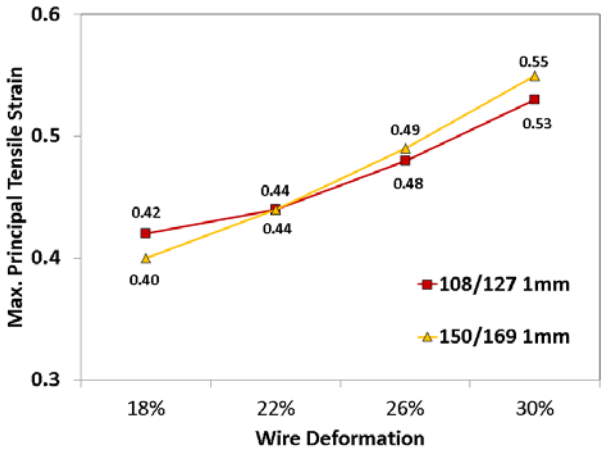


Fig. 11. Maximum principal tensile strain in the wire cross section for the 1 mm 150/169 and 108/127 [4] strand designs as function of wire deformation.

The 150/169 and 108/127 1 mm strands were modeled at 26% wire deformation and the principal tensile strain in the Cu along the 2nd diagonal was plotted in Fig. 10 as a function of radial position. The plastic work per volume follows the same behavior. Because the principal strain increases radially when moving toward the center of the strand, the wire with the additional inner row in principle sees the largest strain. However, the spacing of the subelements in the 150/169 was further increased thereby compensating for that effect. The model was then run for the two designs also at 18%, 22% and 30% deformation levels. Results are shown in Fig. 11, which shows the maximum principal tensile strain found in the cross section as a function of wire deformation. The maximum principal tensile strain in the cross section increases only a little faster with deformation in the 150/169 subelement design than in the 108/127.

### C. *Strand Damage Analysis*

Deformation was applied by a flat roller system to round wires before any reaction. Motorized rollers are used to flatten the strand vertically, and the wire is free to expand laterally. The 150/169 RRP wire of 1 mm diameter was reduced by amounts of 10% to 30% in incremental steps of 5%. At 20%

deformation, the Cu gets thinner in the innermost channels. The Nb-Sn bundles start touching as soon as the Cu channel thickness goes to zero, i.e. breaks, which occurs at 25% deformation, when the Nb starts breaking in the innermost bundles and merging radially outward. Eventually, at 30% deformation, the merging has encompassed the whole thickness of the superconducting area. Fig. 12 shows the number of damaged subelements in each circular row of the superconducting hexagonal area, normalized to the number of cross sections (CS) analyzed, as function of wire deformation.

Fig. 13 plots the number of damaged subelements per cross section found experimentally at each level of deformation for the 1 mm 150/169 and 108/127 strand designs. As can be seen, damage to the Nb-Sn bundles in the 150 subelements design starts at 25% deformation (at which the calculated max. principal strain in the Cu is about the same as that the 108 subelement design deformed at 26%), and a larger fraction of bundles gets damaged once such level is exceeded. This is consistent with the plot of the max. principal strain for the two wires in Fig. 11. As already shown in Figs. 3 and 4, the $I_c$ degradation of the 150/169 wires is negligible up to deformations of 25%, and within 10% up to 30%. However, as shown in Fig. 5, already at the 25% deformation level a reduction in stability current is visible.

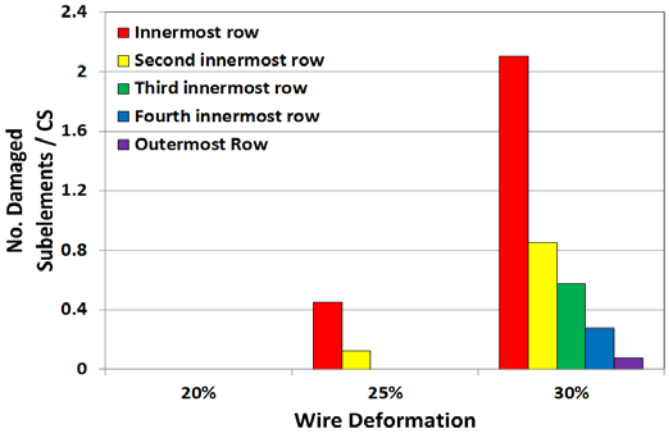


Fig. 12. Number of damaged subelements in each circular row of an RRP wire with 150 Nb-Sn subelements, normalized to the number of cross sections (CS) analyzed, as function of wire deformation.

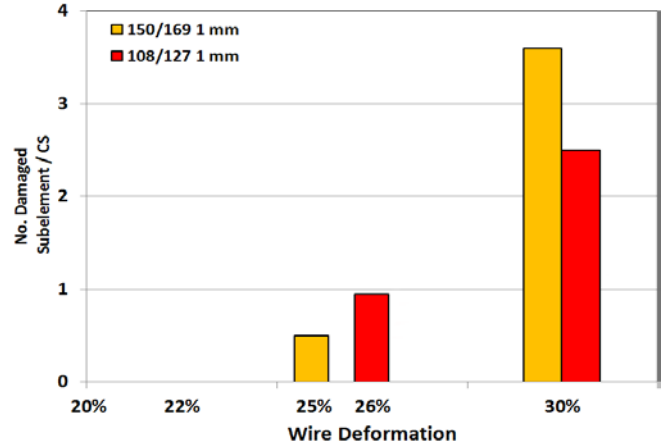


Fig. 13. Number of damaged subelements per cross section found experimentally as function of 1 mm wire deformation for designs with 150 and 108 Nb-Sn subelements.

### *D. Comparison of Strand Performance at 1.9K*

Samples of 0.7 mm 150/169 and 108/127 RRP strands were tested and compared also at 1.9 K. At this temperature the better stability of the 169 restack design is even more apparent than at 4.2K.

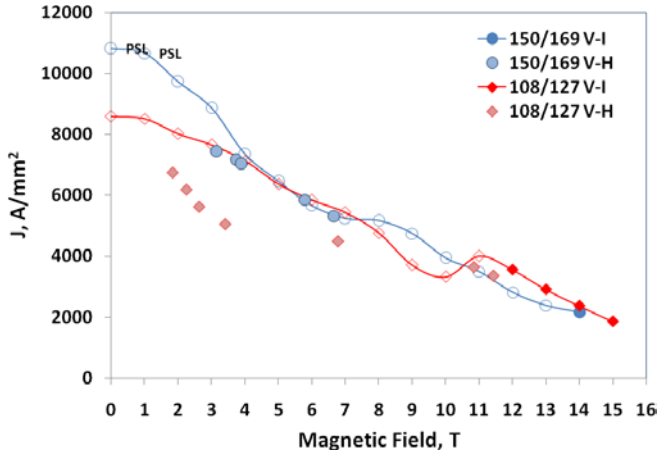


Fig. 14. V-I and V-H test results at 1.9 K for the 0.7 mm strands with 150/169 and 108/127 restacks.

## IV. Conclusion

This study, which compared the effect of increasing deformation on $I_c$, $I_S$ and RRR between the 150/169 and the baseline 108/127 RRP designs, showed the following results. The $I_c$(14 T) degraded similarly or less in the 150/169, and had a systematically better $I_S$ performance both at 4.2 K and at 1.9K. This is consistent with its smaller effective filament size. The 150/169 also had RRR values consistently larger that for the 108/127. ANSYS results of plastic modeling of the two designs were consistent with the microscopic damage analysis.

These coherent results show that the 150/169 design used in this study performed as well as the 108/127 baseline design and was more stable, providing stability margin, which is needed to account for the subelement merging that occur in cables. This design could therefore be used at larger strand sizes.

## References

[1] E. Barzi et al., "Development and study of $Nb_3Sn$ strands and cables for high field accelerator magnets", Advances in Cryogenic Engineering, V. 56, AIP, V. 1219, pp. 183-190 (2010).

[2] H. Felice et al., "Test results of TQS03: a LARP shell-based $Nb_3Sn$ quadrupole using 108/127 conductor", H. Felice et al., 9th European Conference on Applied Superconductivity (EUCAS 2009), Sep. 13-17, 2009, Dresden, Germany.

[3] E. Barzi et al., "Effect of Subelement Spacing in RRP $Nb_3Sn$ Strands", Advances in Cryogenic Engineering, V. 54, AIP, **V. 986**, p. 301-308 (2008).

[4] E. Barzi, M. Bossert, and G. Gallo, "A Model to Study Plastic Deformation in $Nb_3Sn$ Wires", IEEE Trans. Appl. Sup., V. 21, No. 3, p. 2588 (2011).